Mem. S.A.It. Vol. 95, 124

Memorie della

Time-dependent High-Energy Stellar Radiation and Planetary Atmosphere interaction

(THE StellaR PAth)

A. Maggio[1], A. S. Bonomo[2], F. Reale[1,3], C. Argiroffi[1,3], C. Cecchi Pestellini[1], S. Colombo[1], G. Guilluy[2], D. Locci[1], G. Micela[1], S. Orlando[1], A. Petralia[1], I. Pillitteri[1], A. Sozzetti[2], V. Andretta[5], G. Bruno[4], A. F. Lanza[4], I. Pagano[4], P. Pagano[1,3], and G. Peres[1,3]

[1] INAF – Osservatorio Astronomico di Palermo, piazza del Parlamento 1, I-90134 Palermo, Italy. e-mail: antonio.maggio@inaf.it
[2] Osservatorio Astrofisico di Torino, Via Osservatorio 20, I-10025 Pino Torinese, Italy
[3] Dipartimento di Fisica e Chimica, Università degli Studi di Palermo, piazza del Parlamento 1, I-90134 Palermo, Italy
[4] INAF – Osservatorio Astrofisico di Catania, Via S. Sofia 78, I-95123, Catania
[5] INAF – Osservatorio Astronomico di Capodimonte, Salita Moiariello 16, I-80131, Napoli

Received: 26 March 2024; Accepted: 15 July 2024

Abstract. "THE StellaR PAth" project aimed to the development of a composite modeling framework for investigating the effects of time-variable high-energy irradiation on the evolution of exoplanetary atmospheres. Stellar X-UV emission was modeled using the Sun as a scalable template, taking into account variability on different time scales. We applied this radiative input to assess the rate of planetary evaporation, and to model the atmospheric photochemistry. Finally, synthetic transmission spectra were produced to identify spectral diagnostics of chemical species affected by high-energy irradiation, to be probed with NIR spectrophotometry by the ESA M4 space mission ARIEL. As a corollary, entangling of magnetic structures in the solar corona and possible Star-Planet Interactions were also studied through 3D MHD simulations to investigate their relevance in peculiar extra-solar contexts.

Key words. Stars: Stellar Activity – Exoplanets: Atmospheres – X-rays: stars – Extreme UltraViolet: stars – Star-Planet Interactions – Space Mission: ARIEL

1. Introduction

Intensive searches of extrasolar planets in the last few decades, with ground-based and space-based facilities, have already demonstrated that planet formation is ubiquitous in our Galaxy, and extrasolar systems show a surprising variety of properties (Deeg &

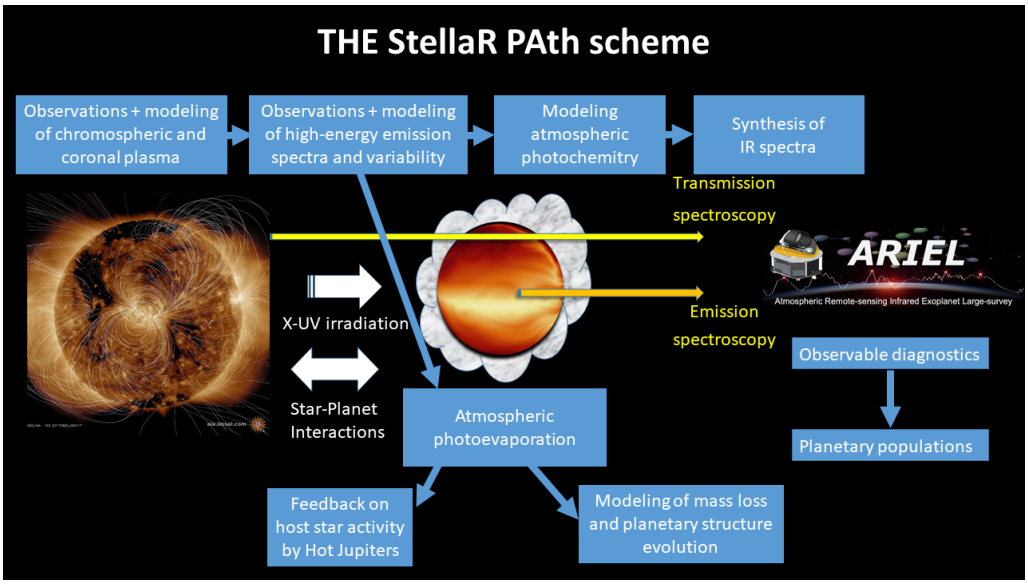

Fig. 1. Schematic illustration of the project rationale, modules, and future scopes with the ARIEL mission.

Belmonte 2018). Multi-wavelength photometry and spectroscopy are routinely employed since a few years to probe the structure, dynamics and chemical composition of planetary atmospheres. In particular, medium and high-resolution transmission spectroscopy in the Near InfraRed (NIR) has been demostrated to be a powerful technique for detecting molecular features in the atmospheres of transiting exoplanets (e.g. Tsiaras et al. 2018; Giacobbe et al. 2021), as well as tracers of atmospheric evaporation such as the He I triplet at 1083 nm (Spake et al. 2018; Nortmann et al. 2018; Allart et al. 2018). New space instrumentation in the IR band is now under development and will fly on board ARIEL, the ESA M4 mission (Tinetti et al. 2018), for the systematic study of exo-atmosphere. The final aim is to assess habitability conditions for planets in "Goldilocks zones" (Kasting et al. 1993), or the possible lack of them for planets embedded in harsh radiation and particle environments.

What is still missed is a comprehensive modeling framework that may allow us to interpret the observations as a result of the forcing effect of stellar irradiation, and to link the atmospheric characteristics with the evolutionary phases of star-planet systems. In fact, diverse spectral components of the stellar irradiation are key ingredients to determine the equilibrium temperature at the planet surface, the scale height and thermodynamic profile of the atmosphere, the mixing ratios of chemical species, and the mass loss rate due to photoevaporation.

In particular, stellar activity, including high-energy emission, flares and coronal mass ejections, may affect profoundly the chemistry and even the retention of planetary atmospheres (Micela 2018).

The present project aimed to develop modeling and analysis tools for interpreting current and future observations, with special attention on solar-type stars across various evolutionary stages. Figure 1 shows a schematic representation of the project rationale and final scopes. At the core of our modeling framework there are two independent modules for the atmospheric photochemistry and photoevaporation, linked by a self-consistent treatment of the XUV (1.24–1800 Å) irradiation of exoplanets.

To this aim, the first step was the modeling of the spectral shape and long-term vari-

ability of the radiation which originates from hot plasma in the stellar outer atmospheres. Our understanding of the evolution of magnetic activity in the chromosphere and corona of the Sun and solar-like stars was a well-suited starting point (Maggio et al. 1987; Ribas et al. 2005). Moreover, we based our approach on the knowledge that the Sun could be employed as a scalable template to predict the global behavior of low- and intermediate-activity late-type stars (Drake et al. 2000; Peres et al. 2004), although there were only few applications of these paradigm to other stars (Favata et al. 2008; Orlando et al. 2017) at the time of the proposal for this project (2019).

The stellar high-energy emission drives the heating and photoevaporation of the planetary atmospheres, especially at young ages and for planets in short-period orbits (Penz et al. 2008; Sanz-Forcada et al. 2011a; Salz et al. 2015, 2016). Modeling of these effects throughout the stellar lifetime is required to reconstruct the evolutionary history of exo-planets in the radius vs. mass diagram, and to interpret spectroscopic proxies of atmospheric mass loss, such as absorption in the stellar Lyα wings (FUV) (Oklopčić & Hirata 2018) or the detection of the NIR He I triplet during planetary transits (Allart et al. 2018; Nortmann et al. 2018; Spake et al. 2018).

High-energy irradiation is also responsible for the photochemistry in planetary atmospheres (Moses et al. 2011; Venot et al. 2018), that can be probed with Earth-based high-resolution spectroscopy or even with space-based instrumentation at lower resolution. In this respect, our project aimed to the development of a new model which included a detailed description of the XUV ionizing radiation field, with the production of primary and secondary electron cascades, and the consequent radiation chemistry. The final aim of the project was the synthesis of the low-resolution NIR spectra that will be gathered by the future ARIEL mission.

Together with the development of predictive models, this project included also the analysis of existing data for the selection of benchmark study cases, and the optimization of target samples for current and future space missions. In this respect, this project was carried on in synergy with a long-term observing program (PI G. Micela) with the HARPS-N and GIANO-B high-resolution spectrographs at the Telescopio Nazionale Galileo (TNG), in the framework of the Global Architecture of Planetary Systems (GAPS) collaboration (Covino et al. 2013; Carleo et al. 2020). Follow-up observations of selected targets at UV and X-ray wavelengths were proposed and carried out as well, as part of HST and XMM-Newton AO programs, because of the need to test and calibrate empirical scaling laws, proposed in literature (Sanz-Forcada et al. 2011a; Chadney et al. 2015; King et al. 2018), that allow to predict the stellar EUV flux (100–920 Å) from measurements in the X-ray band (5–100 Å).

In the following, we illustrate the activities and the main results of the three Work Packages of the project: Modeling of Solar and Stellar Coronae (WP1, Sect. 2), Stellar High-energy Emission, Star-Planet Interactions (SPI), and Planetary Atmospheres (WP2, Sect. 3), NIR Spectroscopic diagnostics (WP3, Sect. 4). We draw conclusions and future prospects in Sect. 5. Deliverables of the project, cited below, were all gathered in a Zenodo archive at the following address: zenodo.org/communities/the-stellar-path.

2. Solar and stellar coronae

Within the scope of this first Work Package, two modeling methodologies were developed: (i) Analysis and interpretation of X-ray spectroscopic observations of stellar coronae using the solar corona as a scalable model (X-ray stars as a scaled X-ray Sun), with applications to data obtained with space-borne high-energy spectrographs (in particular XMM-Newton). (ii) Simulations with time-dependent 3D MHD models of interacting magnetic structures in the solar corona, applied to the interpretation of spectrophotometric measurements of high-energy solar emission, obtained with space instrumentation (in particular the Solar Dynamic Observatory).

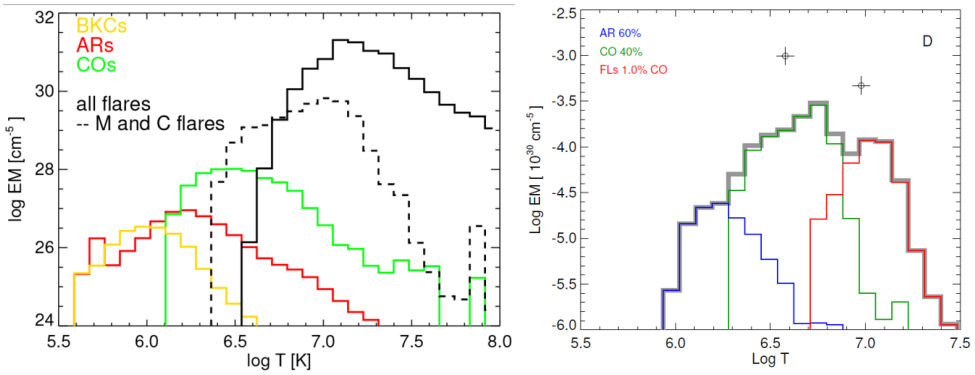

Fig. 2. Left: Average EMDs per unit surface area for each type of magnetic structure observed with Yohkoh: background corona (BKC), active regions (AR), cores (CO), and flares. Right: EMD constructed with the solar components that best match the observations of ϵ Eri. The plus symbols indicate the best-fitting parameters of the X-ray spectra with 2-component thermal models. Adapted from Coffaro et al. (2022).

2.1. Stars as scaled X-ray Suns

The first methodology is based on past studies of the solar corona (Peres et al. 2000; Orlando et al. 2004; Peres et al. 2004; Argiroffi et al. 2008) which allow to describe the X-ray emission of the Sun as the sum of various components of hot plasma (Background corona, Active Regions, Cores of Active Regions, and Flares). For each of these, an Emission Measure Distribution (EMD) of the plasma as a function of temperature was derived (Fig. 2, left panel). The high-energy emission of the Sun, in different phases of the magnetic activity cycle, can be synthesized by an appropriate weighted combination of these components. Reversing the approach, we performed studies on stars similar to the Sun, which host extrasolar planetary systems, observed in X-rays with the XMM-Newton satellite. The spectral analysis allowed the interpretation of the stellar coronal emission as due to a sum of hot plasma components similar to those present in the solar corona, but with different weights.

On the Zenodo platform, we have published the EMD(T) of the various solar components, along with a tutorial for building models of stellar coronae with different levels of activity, characterized by different surface coverage factors of the various components and by different percentages of active regions in flaring phase. The global EMD(T), the sum of all appropriate components, can be used for the interpretation of stellar magnetic activity and the synthesis of X-ray spectra in different energy bands or instrument resolutions. These spectra can then be further used as input for photochemical and photoevaporation models of irradiated planetary atmospheres, and they also take into account statistically the dynamic components of the coronal emission, variable over short time scales.

In the framework of THE StellaR PAth project, we mention in particular the application of this methodology to two stars more active than the Sun (ϵ Eri, in Fig. 2, and Kepler 63), observed at different epochs, which indicated the presence of a surface coverage of active regions cores and flares significantly higher than in the Sun (Coffaro et al. 2020, 2022a,b).

2.2. Magnetic loop interactions in the solar corona

As a second objective, we modeled interacting magnetic structures in the solar corona, observed with the Solar Dynamic Observatory (SDO) satellite. These are phenomena of magnetic reconnection and coronal heating that occur in active regions with various dynamically

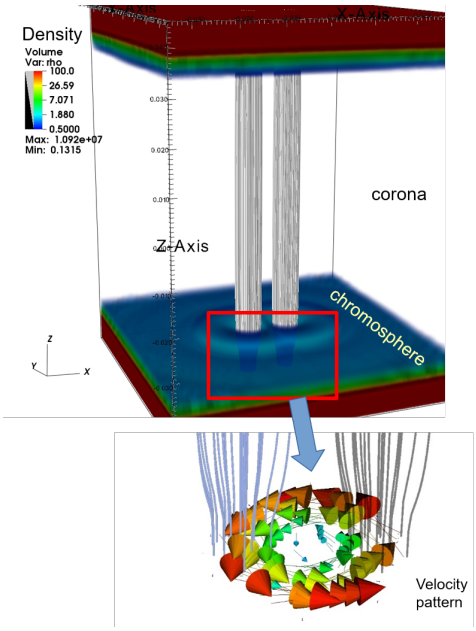

Fig. 3. Schematic view of the 3D MHD simulations of interacting solar magnetic flux tubes.

evolving coronal magnetic arches (Reale et al. 2019a,b). Analyses of micro-flares in the solar corona, observed with SDO/AIA and with Hinode/EIS, showed that these events can be the result of the interactions of magnetic structures, as introduced above. The associated phenomena of magnetic reconnection can produce local heating of the plasma up to temperatures greater than ∼ 10 MK. 1D hydrodynamic models have allowed us to describe a coherent scenario of a system of magnetic loops that give rise to these micro-flares, providing constraints on the intensity of the energy released and on its spatial and temporal distribution (Testa & Reale 2020).

Subsequently, we performed 3D MHD simulations, aimed at demonstrating that the observed phenomena can be described by a system of magnetic field lines that are intertwined by the motions of high-β plasma at the feet of the coronal arches (Fig. 3; Petralia et al. 2024).

The probability of this interaction of magnetic structures increases as the surface coverage factor of the active coronal regions increases. This is therefore a possible component of radiative emission from hot plasma, with a dynamic temporal evolution, which becomes relevant in stars much younger and more active than the Sun, where the coverage factor exceeds 60% (as in the cases of ϵ Eri and Kepler 63 in Sect. 2.1).

3. Stellar high-energy emission, planetary atmospheres, and SPI

Within the scope of this WP, the following four modeling studies were conducted in parallel: (i) Synthesis of spectra in the entire XUV spectral band (1.24–920 Å) for stars with different magnetic activity levels, parameterized by the value of the surface X-ray flux, measurable with space instrumentation. (ii) Improvement and application of a model of photoevaporation of primary atmospheres (dominated by hydrogen and helium), taking into account variations of the planetary equilibrium temperature and of the stellar XUV irradiation over evolutionary timescales. (iii) Updating, implementation, and testing of a model for the photochemistry in planetary atmospheres subject to high-energy radiation. (iv) Time-dependent 3D MHD simulations of magnetic Star-Planet Interactions (SPIs), with reference to extra-solar systems with Jovian planets in tight orbit (Hot Jupiters).

3.1. Stellar XUV spectra

Our approach for the synthesis of stellar XUV spectra is based on distributions of the plasma emission measure vs. temperature, EMD(T), similar to those of the solar corona. To achieve this result, we carried out observational campaigns of selected young active stars (DS Tuc, V1298 Tau, HIP 67522), which host planetary systems, observed both from the ground (Ca II HK chromospheric line emission) and from space with XMM-Newton (soft X band, 1.8–40 Å) and HST (FUV band, 1140–1440 Å). These observations allowed us to test and calibrate scaling laws, previously proposed in the literature, that link the flux in the EUV band (100–920 Å, not directly observable) to the measurable flux in X-rays (5–100 Å, Fig. 4; Maggio et al. 2023).

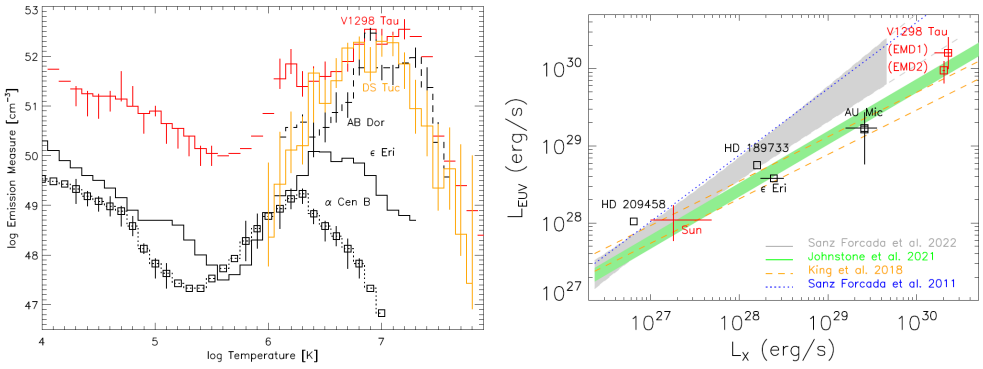

Fig. 4. Left: Plasma EMDs vs. temperature reconstructed for stars with different activity levels. Right: Comparison of different X-ray (5–100 Å) to EUV (100–920 Å) luminosity scaling laws (see labels) with measurements for V1298Tau, the Sun, and other benchmark stars with exoplanets. The gray band indicates the 95% confidence region of the Sanz-Forcada et al. (2022) scaling law. The green band spans over stars with radii in the range 0.7–1.3$R_\odot$, according to Johnstone et al. (2021). The blue dotted line represents the old SF11 scaling law, while the orange dashed lines refer to King et al. (2018).

As a by-product of this observational activity, we have developed a methodology to extend the EMD(T) from the coronal temperature range 10^6–10^7 K down to chromospheric temperatures ($\sim 10^4$ K). In this way, we are able to synthesize emission spectra over the entire XUV band, and hence to model properly the irradiation of planetary atmospheres.

3.2. Atmospheric photoevaporation

As a second objective within the scope of WP2, we updated the model of photoevaporation of planetary atmospheres by Locci et al. (2019), taking into account both the stellar evolution in the temperature–luminosity diagram and the temporal evolution of the X-ray and EUV irradiation over long timescales (on the order of Gyr).

The workflow of this time-dependent photo-evaporation model is schematically illustrated in Fig. 5. At each time step in our simulations, we describe the planet with a core–envelope structure, where the envelope can evolve in response to gravitational contraction and hydro-dynamic escape. The mass loss rate was initially evaluated with the analytic approximation by Kubyshkina et al. (2018). Due to relevant uncertainties and limitations of this

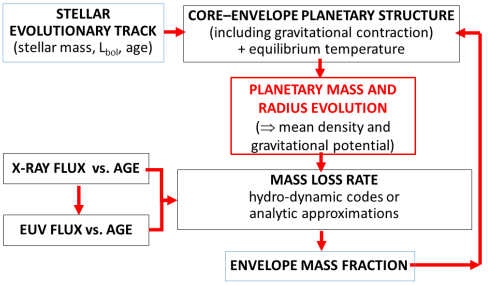

Fig. 5. Schematic workflow of the time-dependent photo-evaporation model.

approach, we eventually adopted the results of the hydro-dynamic code by Caldiroli et al. (2021, 2022). This code solves the hydrodynamics and photoionization equilibrium equations in XUV-irradiated H/He atmospheres, including collisional excitations and ionizations, recombination, and radiative cooling. It allows to determine thermodynamic profiles in planetary atmospheres and the efficiency of photoevaporation which enters as a factor of the classical energy-limited approximation (Erkaev et al. 2007).

For the evolution of the high-energy irradiation, we compared various scaling laws, already proposed in the literature, which describe the time variation of the X-ray emission

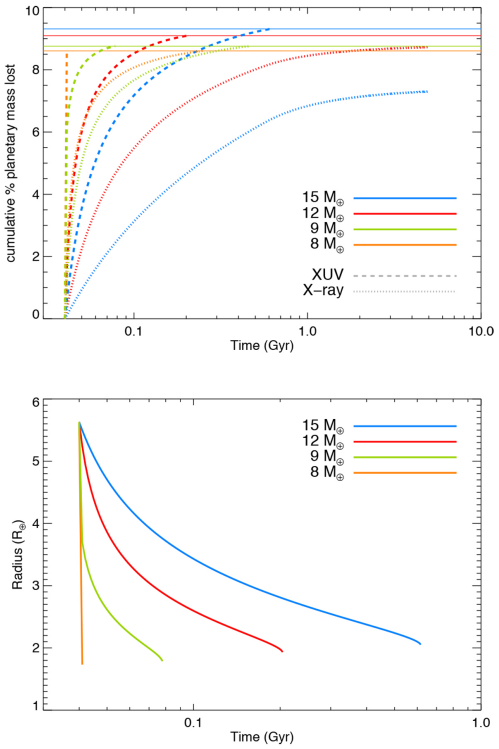

Fig. 6. Upper panel: Cumulative percentage of planetary mass lost by the DS Tuc A b planet vs. age, for different starting masses (color coded, as in the legend). The evolution from the present age to the end of the photoevaporation phase was computed considering the X-ray irradiation alone (dotted lines) or the full X-ray + EUV spectrum (dashed lines). Horizontal solid lines represent the limits of the respective atmospheric mass fractions. Lower panel: Evolution of the planetary radius for the same representative cases as above. Adapted from Benatti et al. (2021).

level (Penz et al. 2008; Johnstone et al. 2021), and others that allow to estimate the integrated EUV emission by means of a power law relationship with the X-ray emission (Sanz-Forcada et al. 2011b; Johnstone et al. 2021).

This model was used to describe the evolutionary history of transiting planets around young stars, recently discovered by means of observations with the Kepler and TESS satellites, and selected within the GAPS program with HARPS-N@TNG dedicated to "Young Objects". In particular, our model allowed us to evaluate the past and future evolution of the masses and radii of selected planets due to photoevaporation induced by XUV irradiation: DS Tuc A b (Benatti et al. 2021; GO program with HARPS@ESO 3.6m telescope), V1298 Tau b, c, d, e (Maggio et al. 2022), HD 63433 b, c (Damasso et al. 2023), TOI-1853 b (Naponiello et al. 2023), TOI-5398 b, c (Mantovan et al. 2024a,b), and TOI-837 b (Damasso et al. 2024). Figure 6 illustrates the specific case of DS Tuc A b, a young (age $\sim$ 40 Myr) Sun-like star which hosts a transiting planet of mass $\leq 15 M_{\oplus}$.

Further X-ray observations with XMM-Newton of the star DS Tuc have allowed us to characterize intense flares with high-energy emission strongly variable over time (Pillitteri et al. 2022a). The TESS light curves of this system were also analyzed, and allowed us the determination of the frequency of flares in the optical (Colombo et al. 2022a). DS Tuc represents therefore an ideal case for the study of the effects of the irradiation from a young solar-type star on the photochemistry of the atmosphere of a (sub-)Neptune-like planet, taking into account the short-term variability due to energetic events.

3.3. Atmospheric photochemistry

A further achievement of our study was the development of a one-dimensional thermochemical and photochemical kinetics model of planetary atmospheres (Locci et al. 2022), taking into account the XUV irradiation, for investigating possible non-equilibrium effects that can be probed by means of NIR spectroscopic observations of transiting planets, from Earth or space.

The model is characterized by an inventory of 68 chemical species, in both the forms of neutrals or ions, including five elements: H, He, C, N, and O. The adopted chemical network of 1978 reactions is available in the Zenodo archive. It contains bimolecular, termolecular, thermodissociative, ion–neutral, and photochemical reactions. The latter include photodissociations, mainly due to UV and EUV radiation, and photoionizations by EUV radiation and X-rays.

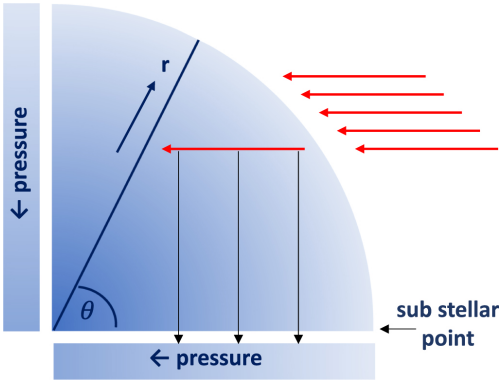

Fig. 7. Geometry of the radiation transfer in the photochemistry model. The incoming radiation travels horizontally, and the zenith angle θ identifies the radial path along which the chemistry is computed. The vertical black arrows indicate the pressures sampled along the photon path. (Adapted from Locci et al. 2022).

Subsequently, the model also takes into account the effects due to primary and secondary electrons. The number distribution of secondary electrons depends on the inverse of the mean energy per ion pair, W, which is the initial energy of the photoelectron divided by the number of secondary ionizations produced as the particle comes to rest. This is computed as a function of the energy of the primary photoelectron, for different abundance ratios and electronic concentrations (Cecchi-Pestellini et al. 2006).

We also implemented the radiative transfer in the one-dimensional, stratified, cloud-free atmosphere, described with 140 layers, which is illuminated by the stellar photon flux in the range between $\sim$ 1.24 and 4100 Å. Then, we can derived the chemistry along a direction defined by any given zenith angle θ (Fig. 7).

Profiles of the mixing ratios of the various chemical species, obtained with different choices for the stellar irradiation, are available in the Zenodo archive. These profiles show substantial effects in the upper atmosphere, specifically due to high-energy irradiation. The example shown in Fig. 8 is inspired by the actual planetary system of HD 189733 (see below).

This photochemistry model was subsequently used for the synthesis of transmission spectra of planetary atmospheres, in particular in the NIR band of the ARIEL mission and for systems selected in the context of WP3 (Sect. 4).

3.4. Magnetic Star-Planet Interactions

Finally, within the scope of WP2, 3D MHD simulations of star-planet interaction (SPI) have been carried out. In particular, the evolution of material evaporated from the atmosphere of a gas giant planet in a tight orbit around HD 189733 was simulated. HD 189733 is a prototype of the class of magnetically active stars with a massive transiting planet (of the hot-Jupiter type, Colombo et al. 2022b). The analysis of these simulations shows relatively dense and hot material, coming from the evaporating atmosphere of the planet, that is channeled by the stellar magnetic field. This material can give rise to diffuse emission and/or pseudo-flares in the case where the material precipitates onto the star, as indicated by the analysis of numerous X-ray observations of HD 189733 (Pillitteri et al. 2022b). This is a further possible component of stellar magnetic activity, whose importance the project aimed to assess. The evaluation of the observability of this phenomenon is discussed in Colombo et al. (2024).

4. NIR spectroscopic diagnostics

The main objective of WP3 was to select exoplanets to be used as benchmarks for simulations of irradiated atmospheres and synthesis of observables with the ARIEL satellite.

For this purpose, high-resolution NIR spectra obtained with the GIANO-B@TNG spectrograph were analyzed as part of the GAPS program, searching for non-equilibrium atmospheric conditions. In this way, six targets were selected: HD 209458b, HD 189733b, WASP-69b, WASP-80b, WASP-107b, and HAT-P-11b. These hot giant exoplanets cover a relatively large range of equilibrium surface temperatures, and they orbit around stars with different levels of magnetic activity, for which

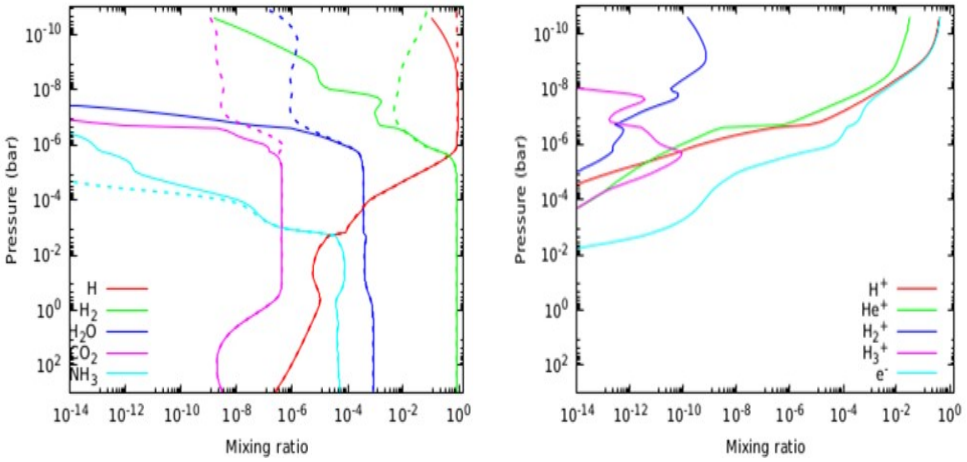

Fig. 8. Vertical density profiles of selected neutral species (left), electrons and ions (left). The solid lines indicate the result of non-equilibrium photochemistry in the atmosphere of a Jovian-mass planet with equilibrium temperature $T_{eq} = 1000$ K, and subject to a XUV flux $\sim 1.3 \times 10^4$ erg s^{-1} cm^{-2}. The dashed lines indicate the distributions if the XUV irradiation is neglected.

the X-ray fluxes are known thanks to archive data from the XMM-Newton mission. In the atmospheres of some of them, the presence of HCN and C_2H_2 molecules has been revealed, which are possible indicators of non-equilibrium conditions due to photochemical processes (Giacobbe et al. 2021; Guilluy et al. 2022a; Carleo et al. 2022; Basilicata et al. 2023). Selection criteria and characteristics of these systems are provided as deliverables of the project in the Zenodo archive.

In particular, the analysis of high-resolution transmission spectroscopy observations of HD 209458b allowed for the first time the detection of six polyatomic molecules in a planetary atmosphere (Giacobbe et al. 2021). Initially, the abundance ratios were largely considered to be compatible with thermochemical equilibrium conditions, but some discrepancies suggested the possibility of non-equilibrium effects as well. A recent combined analysis of the spectra of HD 209458b and HD 189733b, at high resolution with GIANO-B and at low resolution with HST/WFC3, demonstrated the presence of thermochemical disequilibrium in HD 209458b with high statistical significance, but no evidence of it in HD 189733b (Giacobbe et al. 2024, in prep.).

As part of WP3, further work was carried out, as planned in the project proposal, aimed at simulating observations with the ARIEL satellite and predicting planetary evolution due to photoevaporation induced by XUV irradiation. An atmosphere like that on HD 209458b was chosen as a prototype for simulating transmission spectra in different bands and with different resolutions, including all molecular species known from the previous analysis of the GIANO-B NIR spectra (Giacobbe et al. 2021). The TauRex software was used for the synthesis of the ARIEL spectrum (Waldmann et al. 2015b,a; Al-Refaie et al. 2021). This case study showed the possibility of constraining the abundance of HCN but not that of C_2H_2, suggesting the need for a useful synergy between low and high-resolution spectroscopy for reconstructing the characteristics of the transiting planet's atmosphere (Guilluy et al. 2022b).

Subsequently, we developed a new code to calculate NIR spectra in transmission through the atmospheres of giant exoplanets, with the aim of identifying molecular tracers of pho-

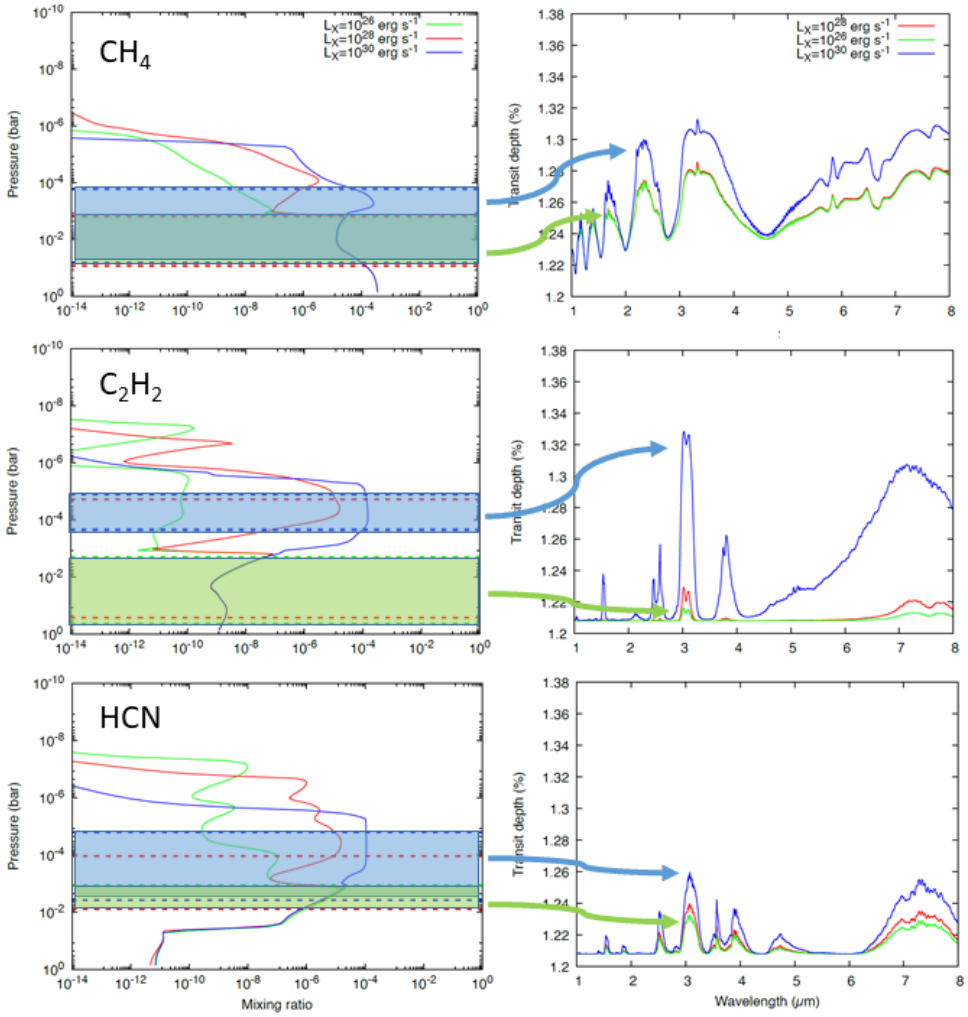

Fig. 9. Vertical density profiles of CH_4 (top left), C_2H_2 (middle left), and HCN (bottom left), for three different levels of stellar XUV irradiation (color coded, as in the legend), and their individual transmission spectra (right panels). Each couple of dashed lines in the left panels indicates the pressure at which the integrated contribution function is comprised between 10% and 90% of the total line absorption, for each species and each irradiation level. The two most extreme cases are shaded in green (lowest XUV flux) and in light blue (highest XUV flux). The corresponding absorption depths, contributed by each species, are shown in the NIR spectra on the right. Adapted from Locci et al. (2024).

tochemical effects due to high-energy irradiation (Locci et al. 2024). This numerical code uses as input the mixing ratio profiles of various chemical species generated by our photochemical model (Sect. 3) and updated cross-sections in the NIR band of interest. In this way, it has become possible to simulate NIR spectra at different spectral resolutions, and in particular spectra in the 1–8 μm band and with the resolution expected for ARIEL (R ~ 300).

The simulations carried out so far show that for stars with high XUV fluxes, photoion-

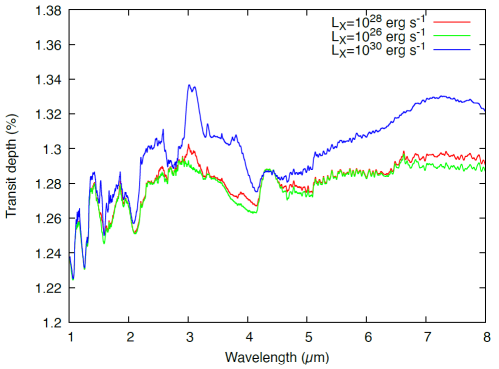

Fig. 10. Total transmission spectra in the ARIEL band, with a resolution R=300, computed by varying the value of the stellar X-ray luminosity, L_x. Adapted from Locci et al. (2024).

ization processes produce spectral signatures mainly due to the molecules of CH_4, C_2H_2 and HCN, which are potentially observable (Fig. 9, and Fig. 10). Effects of non-equilibrium photochemistry were indeed already indicated by high-resolution observations from Earth (GIANO-B@TNG), as anticipated above. The results of our simulations therefore seem to confirm the possibility of these observational diagnostics also with JWST and ARIEL, especially if corroborated by ground-based observations at higher spectral resolution and/or wider spectral band.

Finally, for studying the impact of high-energy stellar radiation on the evolution of exoplanets, we analyzed the He I triplet at 1083 nm. The stellar XUV irradiation plays a dual role in the detectability of this NIR feature: in addition to determining the mass loss rate of the atmosphere, radiation below 50 nm is also responsible for exciting the metastable level that gives rise to the 1083 nm absorption. Observations of this triplet in transmission spectroscopy can be disturbed by the presence of inhomogeneities of the stellar chromosphere, but Guilluy et al. (2020) have shown how to take this effect into account effectively. Consequently, this NIR feature remains one of the most powerful probes of exoplanetary atmospheres (Seager & Sasselov 2000; Oklopčić & Hirata 2018).

This tracer was monitored in several exoplanets, many of which lie on the edge of the hot Neptunian desert. We revealed planetary helium absorption in transmission spectroscopy only in 5 exoplanets, namely HD 189733b, WASP-69b, WASP-107b, HAT-P-11b, and GJ 436b; this indicates that these exoplanets have extended helium atmospheres, in some cases evaporating. On the contrary, for 11 planets only an upper limit was given to the He I line strength, and therefore to the possible loss of atmospheric mass. Our results seem to corroborate previous literature results, according to which the signal of He I absorption is correlated with the stellar mass and the received XUV flux. However, when translated in terms of mass loss rates, it was not possible to identify any statistically significant trend (Guilluy et al. 2024). Furthermore, our unexpected failure to detect He I absorption in WASP-80b (Fossati et al. 2022) poses several challenges to theoretical models of evaporating atmospheres, showing that the mechanisms underlying atmospheric photoevaporation have yet to be fully understood. This empirical evidence has prevented us, up to now, from explaining the dearth of Neptune-sized planets on very short orbits (Period < 4 days), dubbed the hot Neptunian desert (Beaugé & Nesvorný 2013; Owen & Lai 2018), as the result of the evolution of a population of hot giant planets.

5. Discussion and conclusions

Modeling the response of planetary atmospheres to the forcing effect of time-dependent stellar high-energy irradiation requires an adequate understanding of the stationary and dynamic components of the hot plasma in the stellar outer atmospheres. In this respect, our work demonstrates that the Sun can be employed as a scalable template, also for very young stars.

The activity level of individual sources can be reproduced with a proper assembling of solar-like magnetic structures that extend from the chromosphere to the corona, and a proper statistical description of flaring events.

The distribution of plasma emission measure vs. temperature, EMD(T) in the range

$\sim 10^4$–10^7 K, can be derived most accurately from the analysis of X-ray and FUV emission line spectra, taken with instrumentation on board currently available space facilities, such as XMM-Newton and HST. Near simultaneity of these observations is recommended to avoid possible mismatch in different spectral bands due to source variability, but it represents also a strong feasibility constraint.

To overcome this difficulty, the *Stars as scaled X-ray Sun* approach can be adopted (Sect. 2.1), which provides the coronal EMD(T) down to $\sim 10^6$ K. An alternative approach we have devised is based on the work by Wood et al. (2018), who suggested that the coronal EMD(T) can be predicted from the measurement of the stellar surface X-ray flux. An educated guess of the EMD(T) in cromosphere and transition region can be also derived (Maggio et al. 2024, in prep.), by imposing a proper scaling of the integrated EUV flux from the measured X-ray flux, according to the empirical relationships provided by Sanz-Forcada et al. (2022) or Johnstone et al. (2021).

The plasma emission measure distributions provide the best route for predicting the intensity and spectral shape of the stellar high-energy irradiation on exoplanetary atmospheres. The variation of this high-energy flux over long, evolutionary time scales can be predicted with relative accuracy, based on past studies of stellar populations in open clusters, young stellar associations, or in the field (e.g. Penz et al. 2008; Johnstone et al. 2021). The variation on short time scales, from minutes to tens of years, due to impulsive phenomena or magnetic cycles, is more challenging, but it will take advantage from the long-term monitoring of stellar activity with dedicated satellites such as TESS, and PLATO in the near future.

The time-dependent stellar high-energy irradiation is a significant driver of atmospheric photoevaporation, together with internal heating (Ginzburg et al. 2018), at least for Neptune-mass or smaller planets. The evolution of exoplanets with relatively small radii, subjected to strong XUV irradiation and atmospheric photoevaporation, is currently invoked to explain the Fulton gap (or radius valley), i.e. the paucity of exoplanets with radii between $\sim$ 1.5 and $2R_\oplus$ (Fulton et al. 2017). The case of DS Tuc A b (Sect. 3.2) is intriguing in this respect: our simulations (Fig. 11) foresee that this young planet should conclude its evolution in the middle of the Fulton gap, on time scales shorter than 700 Myr.

Our photoevaporation model provides an adequate framework for simulating the evolution of a synthetic population of young planets, with the aim of reproducing the characteristics of the population of mature planets provided by the Kepler and TESS surveys. However this task turned out to be much more complex than expected because our model requires to take into account the stellar and planetary evolution for each system. In particular, in the pre-main-sequence phases, in addition to XUV irradiation, it is also important to evaluate the variation in the planetary equilibrium temperature due to the path of the host star along the evolutionary track, and the variation in the planetary radius due to gravitational contraction. This means that an evolutionary simulation requires a realistic choice of the population of host stars and planets, taking into account both the stellar evolution in the temperature-luminosity diagram and the long-term variation of the XUV emission.

Finally, stellar high-energy irradiation is a crucial driver of photochemistry in atmospheric layers above the planetary thermosphere. Possible departures from thermochemical equilibrium conditions are indicated by our new models (Sect. 3.3 and 4), especially for planets subject to high fluence of X-ray and EUV radiation, i.e. planets in close orbits and/or at young stellar ages (10–100 Myr). Some hints in this direction were already provided by pivotal experiments of transition spectroscopy with Earth-based high-resolution instrumentation (Guilluy et al. 2022a; Carleo et al. 2022), and a detailed comparison with model predictions is on-going, but a much wider sample of cases is required to confirm the observational evidence, and to test for possible variability induced by stellar activity. In this respect, the novel spectroscopic capabilities of JWST and the future ARIEL mission will provide the most adequate database for a

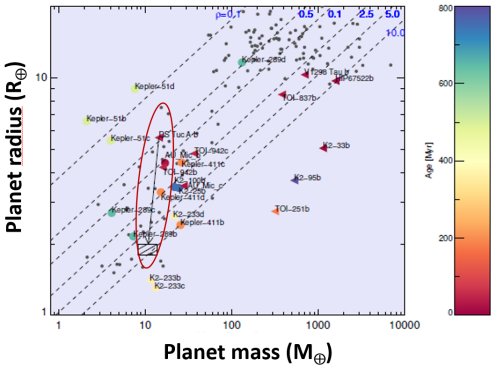

Fig. 11. Planetary mass-radius diagram for a sample of well characterized transiting planets with different ages (see color code). Coloured circles indicate planets with measured mass, while triangles indicate planets with mass upper limit only. Grey dots represent a sample of mature exoplanets. Dashed lines represent loci of equal density, as indicated at the top of the figure. The red ellipse and the hatched rectangle indicate the evolution and final locus of the mass and radius of DS Tuc A b, according to our planetary photoevaporation models (Sect. 3.2). Adapted from Benatti et al. (2021).

complete census of atmospheric characteristics of a variety of extra-solar planetary systems in different evolutionary phases.

Acknowledgements. We acknowledge financial support from the ASI-INAF agreement n.2018-16-HH.0 (THE StellaR PAth project), and from the ARIEL ASI-INAF agreement n.2021-5-HH.0. We also acknowledge partial support by the project HOT-ATMOS (PRIN INAF 2019). GBr acknowledges support from CHEOPS ASI-INAF agreement n. 2019-29-HH.0. This work is based on observations obtained with XMM-Newton, an ESA science mission with instruments and contributions directly funded by ESA Member States and NASA; also based on observations made with the NASA/ESA Hubble Space Telescope, obtained at the Space Telescope Science Institute, and on observations made with the Italian Telescopio Nazionale Galileo (TNG) operated on the island of La Palma by the Fundacion Galileo Galilei of INAF, at the Spanish Observatorio del Roque de los Muchachos of the Instituto de Astrofisica de Canarias.

References

Al-Refaie, A. F., Changeat, Q., Waldmann, I. P., & Tinetti, G. 2021, ApJ, 917, 37
Allart, R., Bourrier, V., Lovis, C., et al. 2018, Science, 362, 1384
Argiroffi, C., Peres, G., Orlando, S., & Reale, F. 2008, A&A, 488, 1069
Basilicata, M. Giacobbe, P., Bonomo, A. S., Scandariato, G., et al. 2023, A&A, submitted
Beaugé, C. & Nesvorný, D. 2013, ApJ, 763, 12
Benatti, S., Damasso, M., Borsa, F., et al. 2021, A&A, 650, A66
Caldiroli, A., Haardt, F., Gallo, E., et al. 2021, A&A, 655, A30
Caldiroli, A., Haardt, F., Gallo, E., et al. 2022, A&A, 663, A122
Carleo, I., Giacobbe, P., Guilluy, G., et al. 2022, AJ, 164, 101
Carleo, I., Malavolta, L., Lanza, A. F., et al. 2020, A&A, 638, A5
Cecchi-Pestellini, C., Ciaravella, A., & Micela, G. 2006, A&A, 458, L13
Chadney, J. M., Galand, M., Unruh, Y. C., Koskinen, T. T., & Sanz-Forcada, J. 2015, Icarus, 250, 357
Coffaro, M., Stelzer, B., & Orlando, S. 2022a, Astronomische Nachrichten, 343, e10066
Coffaro, M., Stelzer, B., & Orlando, S. 2022b, A&A, 661, A79
Coffaro, M., Stelzer, B., Orlando, S., et al. 2020, A&A, 636, A49
Colombo, S., Petralia, A., & Micela, G. 2022a, A&A, 661, A148
Colombo, S., Pillitteri, I., Orlando, S., & Micela, G. 2022b, Astronomische Nachrichten, 343, e10096
Colombo, S., Pillitteri, I., Petralia, A., Orlando, S., & Micela, G. 2024, A&A, 683, A226
Covino, E., Esposito, M., Barbieri, M., et al. 2013, A&A, 554, A28
Damasso, M., Locci, D., Benatti, S., et al. 2023, A&A, 672, A126
Damasso, M., Polychroni, D., Locci, D., et al. 2024, arXiv e-prints, arXiv:2406.08949
Deeg, H. J. & Belmonte, J. A. 2018, Handbook of Exoplanets (Springer International Publishing AG)
Drake, J. J., Peres, G., Orlando, S., Laming, J. M., & Maggio, A. 2000, ApJ, 545, 1074
Erkaev, N. V., Kulikov, Y. N., Lammer, H., et al. 2007, A&A, 472, 329

Favata, F., Micela, G., Orlando, S., et al. 2008, A&A, 490, 1121
Fossati, L., Guilluy, G., Shaikhislamov, I. F., et al. 2022, A&A, 658, A136
Fulton, B. J., Petigura, E. A., Howard, A. W., et al. 2017, AJ, 154, 109
Giacobbe, P., Brogi, M., Gandhi, S., et al. 2021, Nature, 592, 205
Ginzburg, S., Schlichting, H. E., & Sari, R. 2018, MNRAS, 476, 759
Guilluy, G., Andretta, V., Borsa, F., et al. 2020, A&A, 639, A49
Guilluy, G., D'Arpa, M. C., Bonomo, A. S., et al. 2024, A&A, 686, A83
Guilluy, G., Giacobbe, P., Carleo, I., et al. 2022a, A&A, 665, A104
Guilluy, G., Sozzetti, A., Giacobbe, P., Bonomo, A. S., & Micela, G. 2022b, Experimental Astronomy, 53, 655
Johnstone, C. P., Bartel, M., & Güdel, M. 2021, A&A, 649, A96
Kasting, J. F., Whitmire, D. P., & Reynolds, R. T. 1993, Icarus, 101, 108
King, G. W., Wheatley, P. J., Salz, M., et al. 2018, MNRAS, 478, 1193
Kubyshkina, D., Fossati, L., Erkaev, N. V., et al. 2018, A&A, 619, A151
Locci, D., Aresu, G., Petralia, A., et al. 2024, PSJ, 5, 58
Locci, D., Cecchi-Pestellini, C., & Micela, G. 2019, A&A, 624, A101
Locci, D., Petralia, A., Micela, G., et al. 2022, PSJ, 3, 1
Maggio, A., Locci, D., Pillitteri, I., et al. 2022, ApJ, 925, 172
Maggio, A., Pillitteri, I., Argiroffi, C., et al. 2023, ApJ, 951, 18
Maggio, A., Sciortino, S., Vaiana, G. S., et al. 1987, ApJ, 315, 687
Mantovan, G., Malavolta, L., Desidera, S., et al. 2024a, A&A, 682, A129
Mantovan, G., Malavolta, L., Locci, D., et al. 2024b, A&A, 684, L17
Micela, G. 2018, in Handbook of Exoplanets, ed. H. J. Deeg & J. A. Belmonte (Springer International Publishing AG), 19
Moses, J. I., Visscher, C., Fortney, J. J., et al. 2011, ApJ, 737, 15
Naponiello, L., Mancini, L., Sozzetti, A., et al. 2023, Nature, 622, 255
Nortmann, L., Pallé, E., Salz, M., et al. 2018, Science, 362, 1388
Oklopčić, A. & Hirata, C. M. 2018, ApJ, 855, L11
Orlando, S., Favata, F., Micela, G., et al. 2017, A&A, 605, A19
Orlando, S., Peres, G., & Reale, F. 2004, A&A, 424, 677
Owen, J. E. & Lai, D. 2018, MNRAS, 479, 5012
Penz, T., Micela, G., & Lammer, H. 2008, A&A, 477, 309
Peres, G., Orlando, S., & Reale, F. 2004, ApJ, 612, 472
Peres, G., Orlando, S., Reale, F., Rosner, R., & Hudson, H. 2000, ApJ, 528, 537
Petralia, A., Reale, F., Maggio, A., & Testa, P. 2024, in preparation
Pillitteri, I., Argiroffi, C., Maggio, A., et al. 2022a, A&A, 666, A198
Pillitteri, I., Micela, G., Maggio, A., Sciortino, S., & Lopez-Santiago, J. 2022b, A&A, 660, A75
Reale, F., Testa, P., Petralia, A., & Graham, D. R. 2019a, ApJ, 882, 7
Reale, F., Testa, P., Petralia, A., & Kolotkov, D. Y. 2019b, ApJ, 884, 131
Ribas, I., Guinan, E. F., Güdel, M., & Audard, M. 2005, ApJ, 622, 680
Salz, M., Czesla, S., Schneider, P. C., & Schmitt, J. H. M. M. 2016, A&A, 586, A75
Salz, M., Schneider, P. C., Czesla, S., & Schmitt, J. H. M. M. 2015, A&A, 576, A42
Sanz-Forcada, J., López-Puertas, M., Nortmann, L., & Lampón, M. 2022, 21st Cambridge Workshop on Cool Stars, Stellar Systems, and the Sun
Sanz-Forcada, J., Micela, G., Ribas, I., et al. 2011a, A&A, 532, A6
Sanz-Forcada, J., Micela, G., Ribas, I., et al. 2011b, A&A, 532, A6
Seager, S. & Sasselov, D. D. 2000, ApJ, 537, 916
Spake, J. J., Sing, D. K., Evans, T. M., et al. 2018, Nature, 557, 68
Testa, P. & Reale, F. 2020, ApJ, 902, 31
Tinetti, G., Drossart, P., Eccleston, P., et al. 2018, Experimental Astronomy, 46, 135
Tsiaras, A., Waldmann, I. P., Zingales, T., et al. 2018, AJ, 155, 156

Venot, O., Drummond, B., Miguel, Y., et al. 2018, Experimental Astronomy, 46, 101
Waldmann, I. P., Rocchetto, M., Tinetti, G., et al. 2015a, ApJ, 813, 13
Waldmann, I. P., Tinetti, G., Rocchetto, M., et al. 2015b, ApJ, 802, 107
Wood, B. E., Laming, J. M., Warren, H. P., & Poppenhaeger, K. 2018, ApJ, 862, 66